JMEPEG (2008) 17:627–632
DOI: 10.1007/s11665-007-9169-1

1059-9495/$19.00

Simulation of Strength Distribution in Ground Ceramics by Incorporating Residual Stress Effect

Toshihiko Hoshide and Junpei Fujita

(Submitted March 29, 2007; in revised form August 29, 2007)

Strength of ground ceramics may be affected by residual stress as well as surface flaws induced by grinding. Strength prediction for ground ceramics is convenient for mechanical design of ceramic components. In this article, a numerical procedure based on fracture mechanics was proposed to estimate strength distribution of ground ceramics by considering grinding-induced residual stress. Bending strength and residual stress of ground ceramics were measured for three grinding-conditions. By comparison of simulated results with experimental ones, it was revealed that strength characteristics in experiments were well simulated by using the proposed procedure.

Keywords grinding, mechanical testing, Monte Carlo simulation, residual stress, strength estimation, structural ceramics

1. Introduction

Ceramics as sintered materials inevitably include flaws generated in their processing. Pores among grains are formed in binding ceramic powders, and sometimes impure substances are included in mixing powders and additives at the first stage of powder processing. Since most of the ceramic materials shrink after sintering, ceramic parts in functional or structural systems are usually machined to get a specified accuracy of dimension after sintering. Therefore, dangerous flaws in ceramics are also generated during grinding process in addition to sintering process. Considering mechanical design of ceramic parts, preliminary knowledge to achieve the optimization of ceramic strength is efficient in determination of grinding condition. In this situation, some analytical procedures for estimation of ceramics strength are convenient for getting useful information on effects of grinding-induced flaws on ceramic strength. Such analytical procedures should be established on the basis of statistical distributions of flaws, which are generated according to processing conditions in sintering and grinding ceramic materials. It is also noted that residual stress as well as surface flaws are induced by grinding, and they affect strength properties of ceramics (Ref 1-7). The grinding-induced residual stress should be also incorporated in establishing such an analytical procedure.

In this work, a numerical procedure in framework of fracture mechanics was proposed to estimate strength of ground ceramics by taking account of grinding-induced residual stress in addition to flaw distributions. Three-point bending tests were also conducted using silicon nitride ground under several conditions, and the residual stress on ground surface of specimen was evaluated by using an indentation-fracture (IF) method. The applicability of the proposed procedure was discussed by comparing simulated results with experimental ones.

Toshihiko Hoshide and **Junpei Fujita**, Department of Energy Conversion Science, Graduate School of Energy Science, Kyoto University, Sakyo-ku, Kyoto 606-8501, Japan. Contact e-mail: toshi.hoshide@ecs.mbox.media.kyoto-u.ac.jp.

2. Material and Experimental Procedures

2.1 Material

A material to be investigated in this work is a pressureless sintered silicon nitride produced by TOTO Ltd. Physical properties of the material are summarized in Table 1.

2.2 Specimen Preparations

Geometry of the specimen after machining is of a square-rod type with a dimension of 4 mm × 3 mm × 36 mm, which is specified for the standard bending specimen in JIS R 1607 (Ref 8).

Specimens were ground in their longitudinal directions by using grinding wheel of three distinct grit sizes, i.e., #170, #270, and #600. All specimens had been machined using #400 grit wheels before the final grinding as stated above. Using digits of the grit size of grinding wheel, materials ground under the aforementioned conditions are respectively designated SN-170, SN-270, and SN-600. Table 2 summarizes the grinding conditions in this work.

After final grinding, values of centerline average roughness are 0.21 μm for SN-170, 0.20 μm for SN-270, and 0.10 μm for SN-600 in the direction parallel to grinding direction, and 0.88 μm for SN-170, 0.45 μm for SN-270, and 0.17 μm for SN-600 in the direction perpendicular to grinding direction. As a natural result, the roughness in each direction is rougher under coarse grinding-condition in which a wheel of larger grit size is used.

2.3 Bending Test

All bending tests were conducted under three-point bending with a span length of 20 mm, in an ambient atmosphere of 292 ± 2 K and 50 ± 10% in relative humidity. A total of 25 specimens were prepared for each grinding condition. Loading rate was controlled so that the rate of the maximum tensile

Table 1 Physical properties of silicon nitride used in experiment

Density	Fracture toughness, K_{IC}	Vickers hardness	Young's modulus, E	Mean grain size
3.23 Mg/m^3	5.7 MPa m$^{1/2}$	1490 HV50	310 GPa	1.6 μm

Table 2 Grinding conditions

Specimen ID	Grinding wheel	Wheel speed	Table speed
SN-170	SDC170N75BC3.0 (ϕ200 × B15)	25 m/s	0.067 m/s
SN-270	SDC270R100SX6-3.0 (ϕ200 × B25)		
SN-600	SDC600N90BC3-3.0 (ϕ200 × B20)		

stress in a specimen might be about 100 MPa/s. The bending strength of a specimen was evaluated as the maximum stress monitored at its fracture.

2.4 Measurement of Residual Stress by IF Method

As for measurement of residual stress, the X-ray deflection method has successfully been applied in various materials, though alternative simpler methods to estimate residual stress are also required by considering practical and economical needs. For ceramics, especially, a possible candidate for the residual stress estimation is a procedure using IF method (Ref 5, 9-12). A standard based on IF method has been established by the Society of Materials Science, Japan (JSMS). In this work, the JSMS standard (Ref 13), i.e., JSMS-SD-4-01, was adopted to evaluate grinding-induced residual stress. The formula to estimate the residual stress σ_{RO} on a ground specimen surface is expressed as follows.

$$\sigma_{RO} = \frac{K_{IC}(\pi a)^{-1/2} - 0.026(EP/\pi)^{1/2}(d/2)\,a^{-2}}{1.4} \qquad \text{(Eq 1)}$$

In the above equation, material constants K_{IC} and E are respectively the fracture toughness and Young's modulus. Parameters P, d, and a measured in an indentation test are respectively an indentation force, diagonal length of indent and half-crack length on the specimen surface.

Indentation tests in this work were carried out by using a conventional Vickers hardness tester.

3. Experimental Results

3.1 Bending Strength

Figure 1 presents distributions of strength σ_f, which are plotted in a Weibull probability paper. The curved lines in Fig. 1 represent the cumulative probability functions $F(\sigma_f)$, which are fitted to three-parameter Weibull distribution function expressed as

$$F(\sigma_f) = 1 - \exp\left[-\left(\frac{\sigma_f - \sigma_L}{\sigma_S}\right)^m\right] \qquad \text{(Eq 2)}$$

In Eq 2, σ_L, σ_S, and m are respectively location parameter, scale parameter and shape parameter. As expected

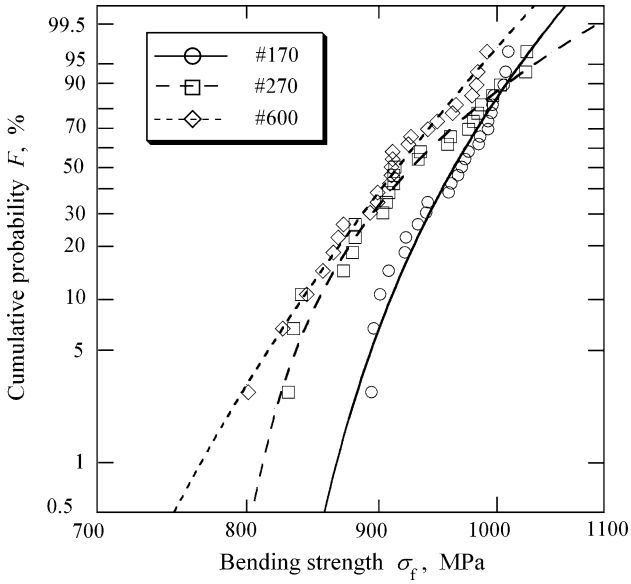

Fig. 1 Weibull plots of strength distributions for three grinding-conditions in experiments

Table 3 Statistics of strength in silicon nitride depending on grinding condition

Specimen ID	SN-170	SN-270	SN-600
Mean strength	961 MPa	929 MPa	911 MPa
Standard deviation	37.5 MPa	58.1 MPa	50.9 MPa
Coefficient of variation	0.0390	0.0625	0.0559
Shape parameter m	30.9	19.5	21.3
Scale parameter σ_S	977 MPa	954 MPa	933 MPa

from the form of Eq 2, each fitted curve in Fig. 1 shows the minimum given by the location parameter σ_L, which is calculated as 797 MPa for SN-170 (indicated with the solid curve in Fig. 1), 779 MPa for SN-270 (the dashed curve in Fig. 1) and 544 MPa for SN-600 (the dotted curve in Fig. 1). As seen in Fig. 1, the strength distribution shifts toward higher strength region for processing by using a grinding wheel of smaller grid number. This implies that rougher grinding results in strength augmentation.

The statistics of bending strength σ_f is summarized in Table 3. Parameters m and σ_S in Table 3 are the shape and scale parameters which are obtained by approximating strength-distribution by two-parameter Weibull distribution function as follows.

$$F(\sigma_f) = 1 - \exp\left[-\left(\frac{\sigma_f}{\sigma_S}\right)^m\right] \qquad \text{(Eq 3)}$$

As seen in Table 3, in the case using rougher wheel in grinding, it appears that the coefficient of variation decreases and the shape parameter increases as a whole trend. This implies that a relative scatter of strength decreases for rougher grinding.

However, it should be noted that the trend mentioned above might be restricted to the case of a combination of material and grinding conditions selected in the present work.

Table 4 Surface residual stress estimated by IF method

Specimen ID	SN-170	SN-270	SN-600
Surface residual stress, σ_{RO}	−80 MPa	−59 MPa	−41 MPa

3.2 Grinding-Induced Residual Stress

The residual stress σ_{RO} on the surface of a ground specimen was measured by JSMS standard using IF method as mentioned above. Vickers indentation tests were carried out by holding 35 s at the maximum indentation force of 490 kN. Measured residual stresses are listed in Table 4. As seen in Table 4, the absolute value of compressive residual stress increases for grinding with wheel of smaller grit number, i.e., rougher grinding.

4. Numerical Simulation of Strength Affected by Grinding Condition

4.1 Basic Model

Inherent flaws generated during a sintering process and grinding-induced flaws are distributed in a specimen. In the simulation, such flaws are modeled as circular, semi-elliptic or quarter-elliptic cracks. Cracks in a specimen are randomly located only within the region, which is subjected to tensile stress in the specimen. It is assumed that the failure of each specimen is dominated by the crack with the maximum stress intensity factor K_{max} among all cracks distributed in the specimen. The fracture stress of one specimen will be determined as the applied maximum stress, at which a calculated value of K_{max} is just equal to the fracture toughness K_{IC} of a material under consideration. Such a calculation is repeated to reach a specified number of specimens. Figure 2 shows the flow chart of the present simulation.

In determining positions of individual cracks, a Cartesian x-y-z coordinate is introduced within the tensile region of a specimen. In this coordinate, x- and y-axes are respectively parallel and vertical to the longitudinal direction of the specimen and z-axis is the transverse direction (width direction) of a specimen (see Fig. 3). By considering no stress gradient in the width direction (z-axis) of specimen under bending mode, positions of cracks existing in an arbitrary cross section are projected in z direction and onto x-y plane. Therefore, in the simulation, the position (x, y) of a crack is prescribed on the x-y plane. For example, the position of i-th crack in a specimen is described as (x_i, y_i) on the x-y plane as shown in Fig. 3. Crack positions are randomly set by using a series of quasi-uniform random numbers generated by a computer. According to crack position, cracks are classified into three types, i.e., embedded, surface, and corner cracks, which are respectively illustrated in Fig. 4. The depth h of the center of an original circular crack is the distance from the specimen surface. The length a and c are radius of an original circular crack and the depth of a modeled crack, respectively.

The size a of each crack is given independently of its location by using a different series of quasi-uniform random numbers. The size distributions for inherent flaw generated during a sintering process and for grinding-induced flaw are respectively expressed by using two distinct functions $F(a)$ of cumulative probability as follows.

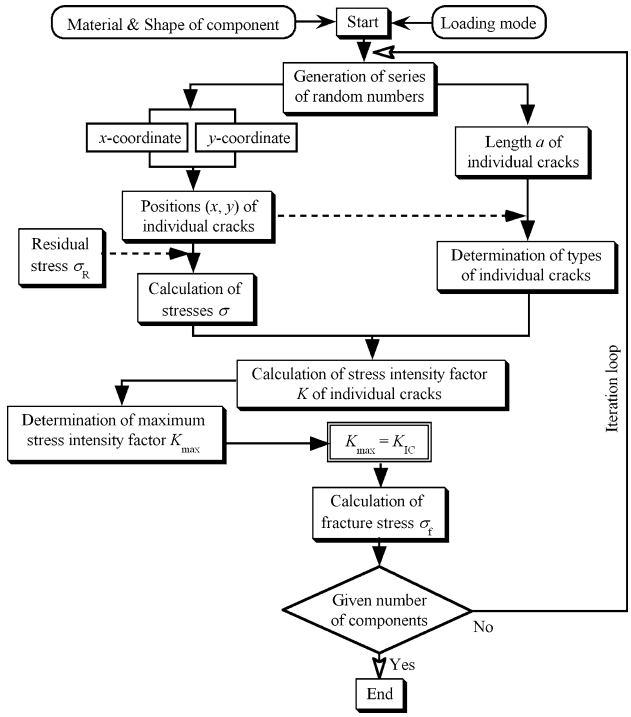

Fig. 2 Flow chart of simulation

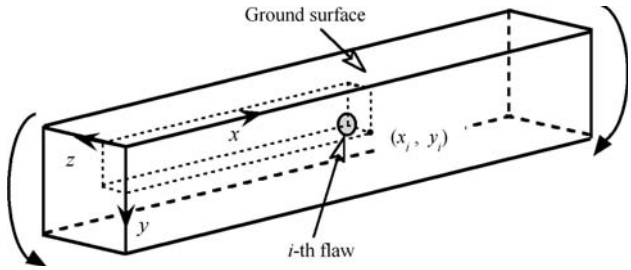

Fig. 3 Cartesian coordinate in specimen subjected to bending

$$F(a_I) = 1 - \exp\left[-\left(\frac{a_I - a_{LI}}{a_{SI}}\right)^{\alpha_I}\right] \quad \text{(Eq 4)}$$

$$F(a_G) = 1 - \exp\left[-\left(\frac{a_G - a_{LG}}{a_{SG}}\right)^{\alpha_G}\right] \quad \text{(Eq 5)}$$

The above equations are of Weibull type with three parameters, i.e., location parameters a_{LI} and a_{LG}, scale parameters a_{SI} and a_{SG}, and shape parameters α_I and α_G. The subscripts "I" and "G" imply crack-size parameters concerned with inherent and grinding-induced cracks respectively.

In this work, the largest size of crack is restricted by considering actual situation that extremely large flaw cannot be observed in dense ceramic materials. The largest size $a_{max,I}$ for inherent cracks is empirically determined as 15 μm based on flaw observations (Ref 14, 17) by a scanning electron microscope. Since surface damage by grinding is much larger than flaws generated during the prior processing and it is difficult to identify actual grinding-damage, the largest size $a_{max,G}$ for grinding-induced cracks is tentatively set to be twice as large as that for inherent ones, i.e., 30 μm. Since the size of

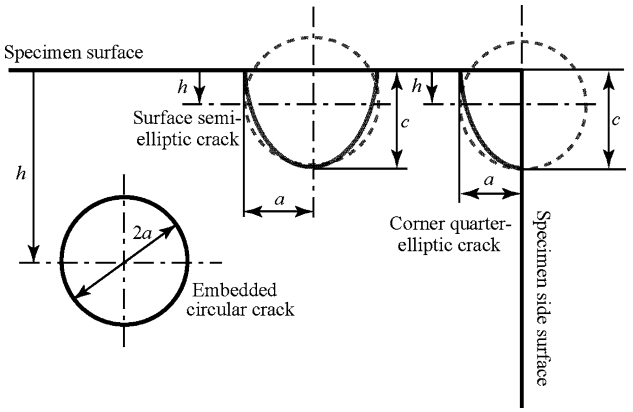

Fig. 4 Schematic illustration of crack patterns

30 μm is so large that the cumulative probability for the appearance of cracks with a size up to 30 μm is 0.999997, there is no substantial meaning for setting the same maximum size irrespective of grinding condition. The crack density depending on grinding condition, if anything, has essential effect on strength in the sense that larger cracks can exist for higher crack density.

It is also presumed that distribution characteristics of inherent crack are common to all specimens. On the other hand, different distributions are assumed for grinding-induced cracks in specimens ground under the respective conditions.

4.2 Fracture Criterion

The simplest fracture criterion of a brittle material is that fracture occurs from a flaw when the stress intensity factor K reaches the fracture toughness K_{IC} of the material. However, it has been reported (Ref 14-17) that such a fracture criterion cannot be directly applied to the strength evaluation of ceramics for the fracture originating from a small flaw; i.e., fracture initiated from a smaller flaw occurs at a lower strength compared with the expected relation between strength σ_f and flaw-size a for a larger crack. In the present simulation dealing with small flaws, the flaw-size dependency of strength as described above should be taken into account in the evaluation of stress intensity factor K for a small flaw so that the evaluated K value can be applied to a fracture simulation based on the fracture toughness criterion. An R-curve model (Ref 18, 19), which expresses grain-bridging effect for longer crack, has been suggested as one of the models to explain such a flaw-size dependency. It has been proposed that a constant δ is added to the original size of the flaw in calculating K value as a simple procedure (Ref 20) to represent such an R-curve behavior. In the present simulation, the approximation is applied to the evaluation of a valid K value for a small flaw as follows.

$$K = \sigma_a \sqrt{\pi(a+\delta)} M_K \qquad \text{(Eq 6)}$$

In the above equation, σ_a is the applied stress, which is determined by loading mode and specimen geometry, and M_K is a magnification factor determined by considering the shape and location of the crack as well as the stress distribution in a specimen. The value of M_K is determined using published numerical results (Ref 21-23) according to the aforementioned situations of crack.

4.3 Incorporating Effect of Residual Stress into Model

The effect of the grinding-induced residual stress is dealt with by superimposing the residual stress on the applied stress in evaluating the stress intensity factor: i.e., the net stress to be replaced with the applied stress σ_a in Eq 6 is given by the summation of the applied stress σ_a and the residual stress σ_R. The net stress intensity factor K_{net} including the residual stress is expressed as

$$K_{net} = (\sigma_a + \sigma_R) \sqrt{\pi(a+\delta)} M_K \qquad \text{(Eq 7)}$$

In bending mode, σ_a has a gradient in the longitudinal (x) and thickness (y) directions.

A grinding-induced residual stress σ_R is generally known to be compressive. In experimental studies (Ref 4-6, 24), it is also reported that the compressive residual stress σ_R has its peak σ_{RO} on or near the ground surface of a specimen and vanishes toward the specimen-depth direction, i.e., the y direction. Such a non-uniform distribution of residual stress in the depth direction should be taken into account in calculating Eq 7. Consider a crack system subjected to a residual stress σ_R given by

$$\sigma_R = \sigma_{RO} f(y) \qquad \text{(Eq 8)}$$

In the above equation, $f(y)$ is a function of depth y that specifies a residual stress distribution. Empirical observations (Ref 12, 13) show that the function $f(y)$ is well approximated by the next equation.

$$f(y) \equiv g(\zeta) = (1 - \zeta^{3.0}) \exp(-3.8109 \zeta^{2.4586}) \qquad \text{(Eq 9)}$$

In the above equation, $\zeta = y/y_0$, and y_0 is the depth at which the compressive residual stress disappears.

4.4 Parameters and Procedure in Simulation

Prior to the actual simulation, preliminary simulations have been carried out for the situation without residual stress. In the preliminary simulations, the combination of parameters to specify the flaw distribution, which are associated with size distribution and density of cracks, are variously changed. As a result by trial and error, parameters have been determined so that the resultant mean strength should be a bit less than the average strength measured for specimens ground by using #600 grinding wheel, which has the lowest residual stress. The density of inherent cracks is defined as the number of cracks per unit volume, while the density of cracks induced by grinding is given as the number of cracks per unit surface area because of the damage which is concentrated on or near the ground surface. It is reasonable to consider that rougher grinding results in larger damage. Therefore, density of grinding-induced crack is increased for rougher grinding, i.e., grinding with a wheel of smaller grit number. The number of surface cracks is given by the crack density and relative crack positions to the specimen surface, though corner cracks and surface cracks are not classified in the analysis. In this simulation, the ratio of corner cracks to total surface ones is empirically determined, and corner cracks are also considered in fracture analysis. Parameters for crack distributions used in the following simulation are listed in Tables 5 and 6.

The depth y_0 is experimentally determined by lapping the ground surface of specimen, and the residual stress is found to disappear by 20 μm lapping. Consequently, in the simulation,

Table 5 Parameters for distribution of inherent crack used in simulation

Density, 1/mm^3	Shape parameter, α_I	Location parameter a_{LI}, μm	Scale parameter a_{SI}, μm	Maximum crack length $a_{max,I}$, μm	Ratio of corner cracks to total surface cracks, %
16	10	5.0	8.1	15.0	1.0

Table 6 Parameters for distribution of grinding-induced crack used in simulation

Wheel grit number	Density, 1/mm^2	Shape parameter, α_G	Location parameter a_{LG}, μm	Scale parameter a_{SG}, μm	Maximum crack length $a_{max,G}$, μm	Ratio of corner cracks to total surface cracks, %
#170	0.32	15	7.0	19.4	30.0	1.0
#270	0.31					
#600	0.30					

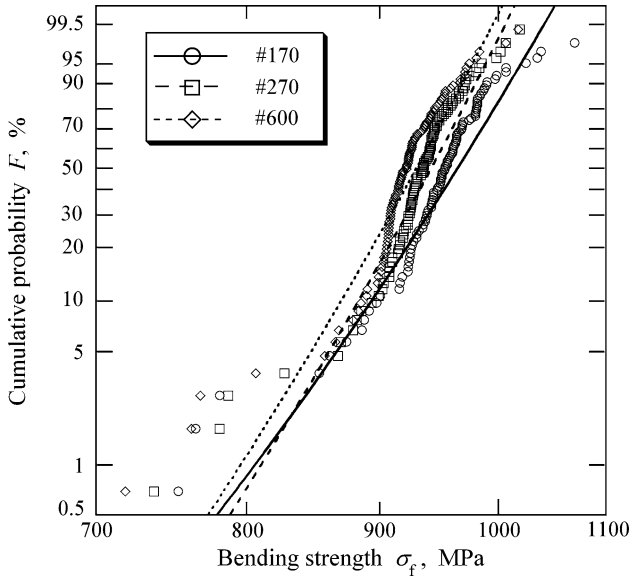

Fig. 5 Weibull plots of simulated strength distributions for three grinding-conditions

y_0 = 20 μm is adopted for the residual stress distribution of Eq 8 and 9.

In the present simulation, a simple procedure to express the *R*-curve behavior is adopted in evaluating *K* value to be valid for a small flaw, and the additional length δ is set to be 6 μm which is found to be appropriate in fitting experimental relations of strength versus flaw-size in the present material (Ref 16).

A Monte Carlo simulation will be carried out for the same shape of specimen under the same loading mode as those adopted in the experiment. In the present simulation, the loop calculation shown in Fig. 2 is iterated 100 times for each grinding condition. Actually, 100 trials are made by creating 100 different combinations of spatial and size distributions of cracks by using random numbers. Consequently, the simulation for each grinding condition gives 100 strength data.

5. Simulated Results and Discussions

A total of 100 strength data simulated for each grinding condition using distinct wheel grit number are plotted in a Weibull probability paper, and the result is shown in Fig. 5. The straight lines in Fig. 5 are strength-distribution relations approximated by two-parameter Weibull distribution functions. Parameters *m* and σ_S are respectively obtained by fitting Eq 3 to simulated strength data for each case. In Table 7, the two parameters in the fitted Weibull distribution functions are listed together with other statistical parameters of strength.

Table 7 Statistics of simulated strength

Wheel grid number	#170	#270	#600
Mean strength	950 MPa	931 MPa	919 MPa
Standard deviation	49.8 MPa	41.0 MPa	42.2 MPa
Coefficient of variation	0.0524	0.0440	0.0459
Shape Parameter, *m*	24.1	28.4	27.6
Scale parameter, σ_S	971 MPa	949 MPa	937 MPa

Figure 5 shows that there is no good fitness of simulated strength data to two-parameter Weibull distribution function. The data plotted under about 880 MPa, in particular, are shifted toward a region of lower strength compared with the relation for other data. In the present simulation, the main crack, which brings about fracture of individual specimen, can be identified by programing. The morphology of crack identified as the main crack can also be found to be inherent or grinding-induced crack, and to be embedded, surface or corner crack. By investigating the relation between crack morphology and strength, it is revealed that strength lower than 880 MPa is dominated by grinding-induced cracks. It should be noted that failure probability in a region of strength lower than 880 MPa is obviously higher than the relation expected in higher strength region. This is considered to be caused by the reduction in restraint by compressive residual stress. Therefore, it is speculated that such grinding-induced cracks in a region of strength lower than 880 MPa are hardly affected by grinding-induced residual stress.

As seen in Table 7, the mean strength is reduced as the wheel grit number becomes larger. In the simulation, as mentioned previously, the density of grinding-induced crack is increased for the case of grinding with smaller wheel grit number, i.e., rougher machining. On the other hand, the absolute value of compressive residual stress is larger in rougher machining as shown in Table 4. Consequently, as for the present combination of material and grinding condition, the improvement effect by inhibition of cracking under

compressive residual stress on strength is more superior to the degradation effect caused by the increase in density of grinding-induced crack.

6. Summary

For prediction of strength of ground ceramics, some analytical procedures are useful in mechanical design of machines or devices using ground ceramic components. Although fracture of ceramic components is generally dominated by inherent flaws, it is noted that, especially in ground ceramics, residual stresses as well as surface flaws are additionally induced by grinding. The grinding-induced residual stress should be also incorporated in establishing analytical procedure. In this work, a numerical procedure in framework of fracture mechanics was proposed to estimate strength of ground ceramics by taking account of grinding-induced residual stress in addition to flaw distributions. To clarify the applicability of the proposed procedure, three-point bending tests were conducted using three kinds of silicon nitride specimens, which were differently prepared by grinding with wheels of three grit-sizes. Grinding-induced residual stress was measured by using an IF method. The bending strength and the absolute value of compressive residual stress were found to increase in grinding with coarser wheel. By comparing simulated results with experimental ones, it was revealed that the increase in strength of ceramics ground with coarser wheel could be well explained by the simulation based on the proposed model. The simulated results suggested that the bending strength was improved by inhibition of cracking under compressive residual stress.

References

1. D. Lewis III, Observation of the Strength of a Commercial Glass-Ceramic, *Ceram. Bull.*, 1982, **61**(11), p 1208–1214
2. H. Fessler, D.C. Fricker, and D.J. Godfrey, A Comparative Study of the Mechanical Strength of Reaction-Bonded Silicon Nitride, *Ceram.-Perform. Appl.*, 1983, **3**, p 705–736
3. M.W. Hawmann, P.H. Cohen, J.C. Conway, and R.N. Pangborn, The Effect of Grinding on the Flexural Strength of a Sialon Ceramic, *J. Mater. Sci.*, 1985, **20**, p 482–490
4. K. Tanaka, K. Suzuki, and Y. Yamamoto, Residual-Stress Effect on Fracture Strength of Ceramics, *Proc. Int. Conf. Residual Stresses*, G. Beck, S. Denis, and A. Simon, Ed., Elsevier Applied Science, 1989, p 15–26
5. T. Hoshide, K. Okumura, and T. Inoue, Experimental Investigation and Numerical Simulation on Bending Strength of Silicon Nitride Affected by Grinding Condition, *J. Soc. Mater. Sci., Japan*, 1991, **40**(449), p 217–233 in Japanese
6. K. Suzuki and K. Tanaka, Residual Stresses and Flaws of Ground Silicon Nitride, *J. Soc. Mater. Sci., Japan*, 1991, **40**(454), p 818–824 in Japanese
7. D.W. Richerson, *Modern Ceramic Engineering Properties, Processing, and Use in Design*, 2nd ed., Marcel and Dekker, Inc., 1992, Chap.12
8. "Testing Methods for Flexural Strength (Modulus of Rupture) of High Performance Ceramics," JIS R 1607, *Japanese Industrial Standard*, Japanese Standards Association, 1995, in Japanese
9. D.B. Marshall and B.R. Lawn, Residual Stress Effects in Sharp Contact Cracking: Part 1 Indentation Fracture Mechanics, *J. Mater. Sci.*, 1979, **14**, p 2001–2012
10. D.B. Marshall, B.R. Lawn, and P. Chantikul, Residual Stress Effects in Sharp Contact Cracking: Part 2 Strength Degradation, *J. Mater. Sci.*, 1979, **14**, p 2225–2235
11. J. Salomonson and D. Rowcliffe, Measurement of Indentation Residual Stresses in Materials Susceptible to Slow Crack Growth, *J. Am. Ceram. Soc.*, 1995, **78**(1), p 173–177
12. T. Hoshide and J. Abe, Grinding-Induced Residual Stress Estimation by Indentation-Fracture Method in Ground Silicon Nitrides, *J. Mater. Eng. Perform.*, 2001, **10**(5), p 586–591
13. "Residual Stress Measurement for Engineering Ceramics by Indentation Fracture Method," JSMS-SD-4-01, *The Society of Materials Science, Japan*, 2001, in Japanese
14. T. Hoshide, H. Furuya, Y. Nagase, and T. Yamada, Fracture Mechanics Approach to Evaluation of Strength in Sintered Silicon Nitride, *Int. J. Fracture*, 1984, **26**, p 229–239
15. T. Hoshide and T. Inoue, Simulation of Anomalous Behavior of a Small Flaw in Strength of Engineering Ceramics, *Eng. Fract. Mech.*, 1991, **38**, p 307–312
16. T. Hoshide, Grain Fracture Model and Its Application to Strength Evaluation in Engineering Ceramics, *Eng. Fract. Mech.*, 1993, **44**, p 403–408
17. T. Hoshide and M. Masuda, Dependence of Strength on Size of Flaw Dominating Fracture in Ceramics, *Mater. Sci. Res. Int.*, 1995, **1**, p 108–113
18. Y.-W. Mai and B.R. Lawn, Crack-Interface Grain Bridging as a Fracture Resistance Mechanism in Ceramics: II. Theoretical Fracture Mechanics Model, *J. Am. Ceram. Soc.*, 1987, **70**, p 289–294
19. R.F. Cook, C.J. Fairbanks, B.R. Lawn, and Y.-W. Mai, Crack Resistance by Interfacial Bridging: Its Role in Determining Strength Characteristics, *J. Mater. Res.*, 1987, **2**, p 345–356
20. T. Hoshide and H. Hiramatsu, A Microstructural Approach to Flaw Size Dependence of Strength in Engineering Ceramics, *Fatigue Fract. Eng. Mater. Struct.*, 1999, **22**, p 1029–1039
21. *Stress Intensity Factors Handbook*, Vols. 1 & 2, Y. Murakami, A. Aoki, N. Hasebe, Y. Itoh, H. Miyata, N. Miyazaki, H. Terada, K. Tohgo, M. Toya, and R. Yuuki, Ed., Pergamon Press, 1987, p 42–45, p 698–711, p 723–724
22. *Stress Intensity Factors Handbook*, Vol. 3, Y. Murakami, M.T. Hanson, N. Hasebe, Y. Itoh, K. Kishimoto, H. Miyata, N. Miyazaki, H. Terada, K. Tohgo, and R. Yuuki, Ed., The Society of Materials Science, Japan, and Pergamon Press, 1992, p 591–597, p 606–610
23. *Stress Intensity Factors Handbook*, Vols. 4 & 5, Y. Murakami, N. Hasebe, Y. Itoh, K. Kishimoto, H. Miyata, N. Miyazaki, N. Noda, C. Sakae, H. Shindo, and K. Tohgo, Ed., The Society of Materials Science, Japan, and Elsevier Science Ltd., 2001, p 570–576, p (A-7)–(A-8)
24. Y. Sakaida, S. Harada, and K. Tanaka, Estimation of Residual Stress Distribution of Ground Ceramics by Gracing Incidence X-ray Diffraction Technique, *J. Soc. Mater. Sci., Japan*, 1993, **42**(477), p 641–647 in Japanese